Experimental investigation of bond behaviour of two common GFRP bar types in high - strength concrete

Najia Saleh, Ashraf Ashour, Dennis Lam and Therese Sheehan
School of Engineering, University of Bradford, Bradford, BD7 1DP, UK
E-mails: N.saleh1@student.bradford.ac.uk, a.f.ashour@bradford.ac.uk, d.lam1@bradford.ac.uk, T.sheehan@bradford.ac.uk

ABSTRACT

Although several research studies have been conducted on investigating the bond stress –slip behaviour of Glass-Fibre Reinforced Polymer (GFRP) bars embedded in high strength concrete (HSC) using a pull-out method, there is no published work on the bond behaviour of GFRP bars embedded in high strength concrete using a hinged beam. This paper presents the experimental work consisted of testing 28 hinged beams prepared according to RILEM specifications. The investigation of bond performance of GFRP bars in HSC was carried out by analysing the effect of the following parameters: bar diameter (9.5, 12.7 and 15.9 mm), embedment length (5 and 10 times bar diameter), surface configuration (helical wrapping with slight sand coating (HW-SC) and sand coating (SC)) and bar location (top and bottom). Four hinged beams reinforced with 16 mm steel bar were also tested for comparison purposes.

The majority of beam specimens failed by pull-out. Visual inspection of the test specimens showed that the bond failure of GFRP (HW-SC) bars usually occurred owing to the bar surface damage, while the bond failure of GFRP (SC) bars was caused due to the detachment of sand coating. The GFRP bars with helical wrapping and sand coated surface configurations showed different bond behaviour and it was found that the bond performance of the sand coated surface was better than that of the helically wrapped surface. Bond strength reduced as the embedment length and bar diameter increased. It

was also observed that the bond strength for the bottom bars was higher than that of the top bars. The bond strength was compared against the prediction methods given in ACI-440.1R, CSA-S806 and CSA-S6 codes. All design guidelines underestimated the bond strength of both GFRP re-bars embedded in high strength concrete.

Keywords: GFRP bar, high strength concrete, hinged beam, bond behaviour and design code

1 Introduction

In the last decades, fibre reinforced polymer (FRP) re-bars have been used as an alternative to the conventional steel reinforcement in concrete structures to overcome the corrosion problem effectively. FRP bars have high corrosion resistance, high tensile strength, light weight and speed of application leading to decreasing construction costs. However, FRP composites suffer from lack of ductility, lower bond strength, lower elastic modulus and higher cost than steel. The bond mechanism between FRP re-bars and concrete is a critical design parameter that controls the performance of reinforced concrete members at serviceability and ultimate limit states. Therefore, several research investigations have taken place to investigate the bond properties of FRP re-bars embedded in concrete.

Most previous studies investigated the bond behaviour of FRP re-bars in concrete using pull-out test method [1-6]. However, very limited experimental data are available in the literature regarding bond behaviour of FRP re-bars in concrete using hinged beams [7-10], as they are more challenging to prepare and test. Despite this, hinged beams are more realistic and representative of stress conditions in RC members in bending than pull-out specimens. Benmokrane et al. [7] tested twelve beams reinforced with helically wrapped GFRP and steel bars in normal strength concrete (NSC). It was found that the bond strengths of GFRP re-bars varied from 6.4 to 10.6 MPa, depending on bar diameter. In addition, the bond strength of GFRP bars was lower (60 to 90 %) than that of steel bars, also depending on bar diameter. It was concluded that as bar diameter increases, bond strength reduces. Tighiouart et al. [8] investigated 64 beams reinforced with GFRP bars having two outer surfaces (spirally wound and deformed), and steel bars. It was reported that the average bond strength was in the range of 5.1 to 12.3 MPa, depending on bar diameter and embedment length. Also, GFRP bars showed bond strength values lower than steel bars. Xue et al. [10] examined 30 unconfined hinged beams reinforced with sand-coated deformed GFRP and steel bars. Experimental results showed that specimens with embedment lengths less than $5d_b$, failed by pull-out, while those with embedment lengths greater than $5d_b$, failed by splitting. Both types of failure were observed in specimens with bonded lengths equal to $5d_b$. It was found that the increase of bar diameter and embedment length resulted in decreasing the bond strength.

In recent years, a marked increase in the use of high-strength concrete (HSC) has been evident in construction projects around the world. HSC offers significantly better structural engineering properties, namely better durability, higher compressive and tensile strengths, higher stiffness compared with conventional normal-strength concrete. The previous studies have focused on investigating the bond behaviour of glass fibre-reinforced polymer (GFRP) bars in normal strength concrete (NSC) [7, 8]. However, no investigation was conducted on high strength concrete hinged beams reinforced with GFRP-SC and GFRP (HW-SC) bars.

Several GFRP bars have been manufactured with various surface configurations (ribbed, helical wrapped, indented and sand coated). However, there is no standardization for surface characteristics, unlike steel bars. Subsequently, the determination of bond properties of each surface is a fundamental requirement for the structural use, because this influences the mechanism of load transfer from concrete to reinforcing bar. Very limited studies were done to investigate the effect of bar surface on bond strength using a hinged beam method. The results obtained by Tighiouart et al. [8] indicated that the ratio of the bond strength for a GFRP deformed surface to that of a GFRP spirally wound surface changed from 1.15 to 1.48 depending on bar diameter. Mazaheripour et al. [11] found that the bond strength of the ribbed GFRP bars is higher than that of the sand-coated GFRP bars embedded in self-compacting steel fibre reinforced concrete. Therefore, this study aimed to examine and compare the bond behaviour of two common GFRP bar types (helical wrapping with slightly sand coating and sand coating).

The literature illustrates that the FRP bar position effect on bond strength was investigated by some authors [8, 12-16]. Tighiouart et al. [8] used the pull-out test to examine the position effect of GFRP (spirally wound) bar in NSC on bond strength. The results showed that the ratio of the bond strengths of the bottom bars to the top bars was in the range between 1.09 and 1.32 with an average of 1.29. In addition, the ratios obtained from the results of pull-out test changed from 1.08 to 1.38 with an average of 1.23 and from 1.11 to 1.22 with an average of 1.18 for NSC and HSC, respectively [12]. Moreover, Ehsani et al. [13] reported that the top modification factor was 1.25 from testing pull-out specimens. Furthermore, Benmokrane and Masmoudi [14] obtained the top modification factor of FRP C-bar equal to 1.1 from pull-out test. The results obtained from testing pull-out specimens revealed that the reduction of water to cement ratio and using high cementitious materials decreased the bond strength variation between the upper and lower zones of the specimens [16]. While, Pay et al. [15] investigated the bar position effect on bond behaviour using lap splice specimens. The results reported that the bond strength of the top-cast specimens is slightly lower (average 7% reduction) than that of the bottom-cast specimens due to lesser water bleeding and concrete slump. However, the effect of bar position on bond strength has not been investigated using hinged beam. Therefore, the current study aimed to investigate the influence of bar position on bond strength. These points are the main motivations to conduct this research and also providing data for designers and code development.

Bond characteristics are influenced by many parameters, such as bar diameter, embedment length, concrete strength, surface configuration, concrete cover and bar position. Experimental investigations were carried out to understand the effect of these factors on bond performance and empirical equations were developed to estimate the bond strength of FRP bars in concrete [2, 8, 13]. However, most equations in the literature included two main parameters: bar diameter and concrete strength, the effect of embedment length, surface configuration, concrete cover, bar position and bar type were ignored. In addition, design guidelines have proposed equations to determine the development length of FRP bars in conventional concrete considering the effect of bar diameter, concrete strength, concrete cover, bar position and bar surface. Canadian codes [17, 18] acknowledge the influence of surface treatment on bond performance by suggesting a bar surface factor in their equations, whereas ACI 440.1R code does not include any special provisions for surface configurations. Moreover, the effect of bar type on bond characteristics was considered in the CAN/CSA-S806 equation only. All codes neglected the influence of transverse reinforcement, except CAN/CSA-S6. The performance of these design equations should be investigated to validate their applicability to high strength concrete reinforced with GFRP (HW-SC) and GFRP (SC) re-bars.

This paper presents the experimental testing of twenty-four GFRP and four steel reinforced concrete hinged beams. The aim of this study is to gain a better understanding of the bond behaviour between GFRP bars and concrete. The bond behaviour is analyzed for GFRP bars with two different surfaces showing the effect of bar diameter, embedment length, surface configuration and bar position on bond strength. In addition, this research aims to validate code equations in the case of high strength concrete.

2 Experimental investigation

2.1 Materials

Hinged beams were constructed using ready – mixed concrete with the maximum aggregate size of 10 mm. Cylinder (150 x 300 mm) and cube (100 x 100 x 100 mm) specimens were cast and cured under the same condition as the test beams. Cylinders and cubes were tested immediately after testing hinged beams to provide the splitting tensile and cube compressive strengths of concrete. GFRP (HW-SC), GFRP (SC) and steel bars were used in this study. The sand coated GFRP and helically wrapped with slightly sand coated GFRP re-bars shown in Figure 1 were made of continuous longitudinal fibres impregnated in vinylester resin: the minimum content of continuous ECR-glass fibres was 75% (per weight) and the maximum content of vinylester resin was 25%, and the content of continuous E-glass fibres 80% (per weight) and vinylester resin 20%, respectively. The tensile strength and elastic modulus of GFRP and steel bars were determined according to specifications ASTM D7205/D7205M [19] and ASTM A706/A706M [20], respectively. The tensile strength of GFRP (SC) bars is higher than that of GFRP (HW-SC) bars as shown in Table 1, due to the difference in the manufacturing process and volume of fibers and resin. However, the tensile strength of GFRP bars would not have a major effect on their bond characteristics with concrete but would have on their development length. The tensile force The actual diameters were measured according to ACI 440.3R-12 [21]. The geometrical and mechanical properties of GFRP and steel bars are summarized in Table 1.

Table 1. Geometrical and mechanical properties of GFRP and steel bars

Bar type	GFRP (HW-SC)			GFRP (SC)			Steel
Bar size	3#	4#	5#	3#	4#	5#	5#
Nominal diameter (mm)	9.5	12.7	15.9	9.5	12.7	15.9	16
Measured diameter (mm)	10.76	13.44	16.76	10.4	13.33	16.74	-
Tensile strength (MPa)	827 (940.2)	758 (797)	724 (867.9)	1227.3 (1224.6)	1375 (1175.4)	1373.7 (1210.3)	672 (666)
Ultimate strain (%)	1.79	1.64	1.57	2.4	2.7	2.7	-
Elastic of modulus (GPa)	46 (51.7)	46 (49.7)	46 (46.9)	50 (50.98)	51 (51.57)	51 (52.15)	200 (199)
Yielding strength (MPa)	-	-	-	-	-	-	582 (569)

The values between brackets measured in the laboratory are the average of three samples, whereas other values are provided by the manufacturer.

(a) Helically wrapped with sand coated surface (type A)

(b) Sand coated surface (type B)

Figure 1. Surface configurations of GFRP re-bars

2.2 Test specimens

Twenty-four GFRP reinforced concrete hinged beams and four steel reinforced concrete specimens were tested. The parameters investigated were bar diameter (9.5, 12.7 and 15.9 mm for GFRP and 16 mm for steel), embedment length (five and ten times bar diameter), bar position (bottom and top) and surface configuration (helical wrapping with slightly sand coating and sand coating). The geometrical details of hinged beams are given in Figure 2. The un-bonded length was covered by a plastic sleeve to prevent contact between the bar and concrete. The presence of confining reinforcement did not appear to influence the bond strength as reported by the ACI 440.1R code [22]. Therefore, the current study has aimed to cast the hinged beams without transverse reinforcement, similar to the specimens of Xue et al. [10] and Mazaheripour et al. [11]. The concrete mix C1 was used to cast twelve specimens reinforced with GFRP (type A) and two steel reinforced concrete hinged beams having embedment length $5d_b$. Specimens reinforced with GFRP (type B) and those reinforced with steel bars having embedment length $10d_b$ were cast using the second batch C2. The test specimens for each bar type were classified into two series: (a) that were cast with the bottom bar position as shown in Figure 2, (b) that were cast with the top bar position as the same as presented in Figure 2, but in an inverted position to make the lower part where the upper part should be. Before casting, the inner sides of the wooden moulds were covered by a thin film of oil to ease demoulding of specimens. The concrete was placed in two layers and each layer was vibrated by using a poker vibrator. After casting, all specimens were covered with polythene sheet to prevent evaporation of water from the unhardened concrete until demoulding. After two weeks, the specimens were demoulded, marked, covered with polythene sheet and stored in the lab temperature until testing.

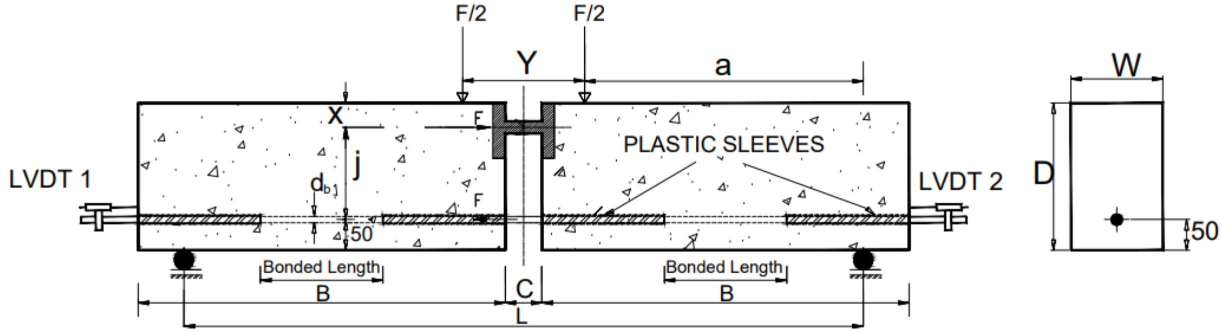

Beam No.	d_b	W	D	L	B	C	X	Y	j
Type I	10-14	100	180	650	375	50	30	150	100
Type II	16-32	150	240	1100	600	60	40	200	150

Figure 2. Hinged beam test arrangement (dimensions in mm)

2.3 Experimental set-up

The beam tests were conducted in accordance with the requirements of the RILEM specification [23]. Specimens consisted of two rectangular concrete blocks joined at the top by a steel hinge and at the bottom by a reinforcing bar to investigate its bond with concrete. The hinged beam was resting on two roller bearings and subjected to two equal forces symmetrically on either side of a ball joint using a testing machine with a capacity of 500 kN as shown in Figure 3(a). Linear variable displacement transducers (LVDTs) were attached to the extended part of the reinforcing bar and held against the concrete end surface to measure the unloaded end slip (accurate to ± 0.025 mm) as illustrated in Figure 3(b). Applied load and LVDT readings were automatically recorded using a data logger. All specimens were tested under displacement control mode so that the post-peak behaviour can be recorded. The loading rate was 0.02 mm/sec and it was kept constant and continuous until complete failure.

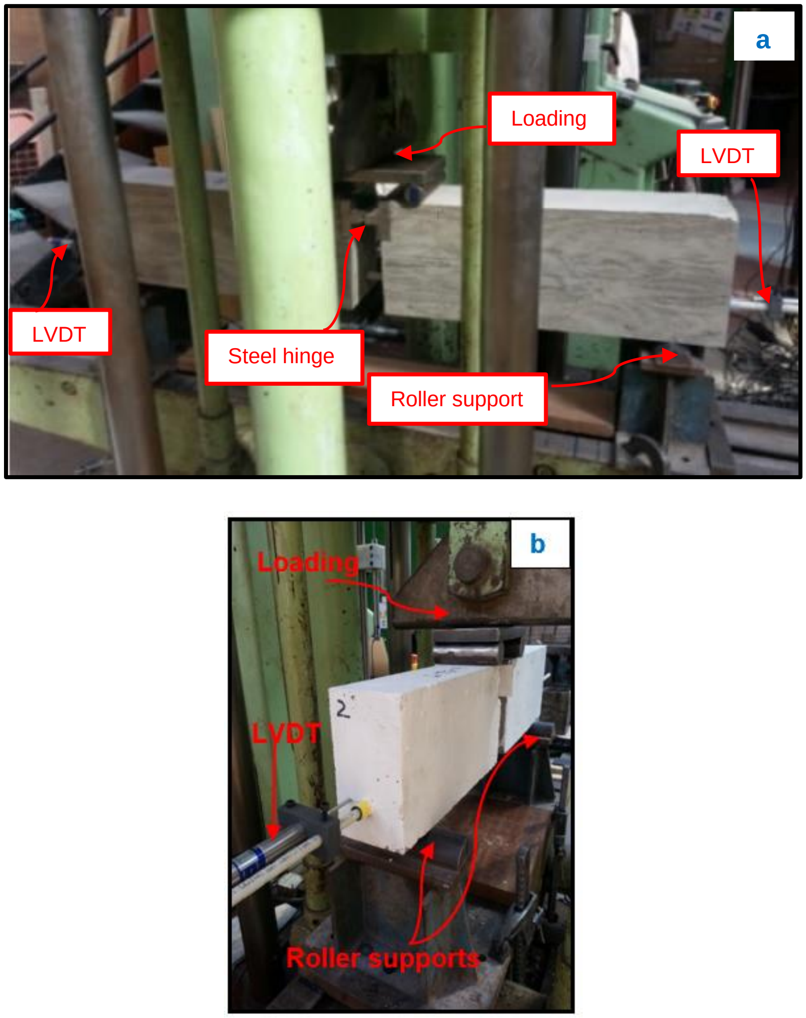

Figure 3. Hinged beam test set-up: (a) front view and (b) side view

3 Test results and discussion

Experimental results were used to develop the bond stress – slip relationships. The tensile load acting on the reinforcing bar can be determined by equilibrium of forces as follows:

For Type I specimens $$T = \frac{\frac{F}{2}.a}{j} = 1.25\,.\,(\mathrm{F}) \qquad (1)$$

For Type II specimens $$T = \frac{\frac{F}{2}.a}{j} = 1.50\,.\,(\mathrm{F}) \qquad (2)$$

The average bond stress could be calculated as presented in the equation below.

$$\tau = \frac{T}{\pi . d_b . l_e} \tag{3}$$

where T is the tensile load in reinforcing bar (N); $\frac{F}{2}$ is the applied load (N); a is the shear span (mm); j is the lever arm (mm); τ is the bond stress (MPa); d_b is the nominal bar diameter (mm) and l_e is the embedment length (mm). The maximum applied load F_{max} (kN), the maximum bond strength (τ_{max}) with the corresponding free end slip (S) are presented in Tables 2 (for type A specimens) and 3 (for type B specimens). The average cube compressive strength of concrete C1 and C2 obtained from testing ten cubes were 97.38 MPa and 81.74 MPa at the testing day of hinged beams, respectively. While the splitting tensile strength of concrete C1 and C2 obtained from testing five cylinders were 4.13 MPa and 3.24 MPa at the testing day of hinged beams, respectively. The definition of beam notation is as follows: the first letter denotes the bar type (A for GFRP (HW-SC), B for GFRP (SC) and C for steel); the first number indicates the bar diameter; the third one denotes the embedment length and the last letter refers to the bar position (B for bottom and T for top bar location).

Table 2 – Bond test results of GFRP (type A) and steel bars in concrete C1

Beam label.	F_{max} kN	τ_{max} MPa	S mm	Failure mode
A-9.5-5d-B	30.56	26.94	0.536	Pull-out
A-9.5-5d-T	29.43	25.94	0.609	Pull-out
A-12.7-5d-B	45.39	22.39	4.426	Pull-out
A-12.7-5d-T	39.95	19.70	11.91	Pull-out
A-15.9-5d-B	55.09	20.80	0.213	Pull-out
A-15.9-5d-T	48.02	18.13	1.176	Pull-out
A-9.5-10d-B	65.49	28.86	0.642	Pull-out
A-9.5-10d-T	59.43	26.19	0.418	Pull-out
A-12.7-10d-B	68.91	16.99	2.33	Pull-out
A-12.7-10d-T	68.18	16.81	1.80	Pull-out
A-15.9-10d-B	82.35	15.55	0.119	Pull-out /Splitting
A-15.9-10d-T	81.41	15.37	0.263	Pull-out /Splitting
C-16-5d-B	69.92	>26.07	0.31	Shear
C-16-5d-T	64.54	>24.06	0.21	Shear

Table 3 - Bond test results of GFRP (type B) and steel bars in concrete C2

Beam label.	F_{max} kN	τ_{max} MPa	S mm	Failure mode
B-9.5-5d-B	33.72	29.72	0.141	Pull-out
B-9.5-5d-T	33.20	29.26	0.11	Pull-out
B-12.7-5d-B	59.78	29.48	0.115	Pull-out
B-12.7-5d-T	49.30	24.31	0.316	Pull-out
B-15.9-5d-B	73.21	27.64	0.104	Pull-out
B-15.9-5d-T	52.22	19.72	0.12	Pull-out
B-9.5-10d-B	64.33	28.34	0.096	Pull-out
B-9.5-10d-T	58.46	25.76	0.1	Pull-out
B-12.7-10d-B	91.11	22.47	0.231	Pull-out
B-12.7-10d-T	83.94	20.70	0.073	Pull-out
B-15.9-10d-B	112.1	>21.16	0.053	Shear
B-15.9-10d-T	83.27	15.72	0.07	Pull-out
C-16-10d-B	109.2	>20.37	0.173	Yielding
C-16-10d-T	105.4	>19.65	0.088	Yielding

3.1 Bond stress – slip relationship

Bond stress – unloaded end slip curves for GFRP (type A) and GFRP (type B) reinforced hinged beams were plotted in Figures 4 and 5, respectively. Figure 6 presents the bond stress – unloaded end slip responses for steel reinforced hinged beams. In general, the bond stress – slip curves of identical specimens with differing bar position only are similar. The bond stress – slip relationships are presented according to bar diameter, embedment length, surface characteristics, bar position and bar type to observe the influence of these main parameters on the bond behaviour in case of high strength concrete.

The general bond stress – slip behaviour is described by a high increase of initial bond stress without a significant slip in both GFRP types because of good chemical adhesion between the bar surface and surrounding concrete. After the chemical adhesion is exhausted, bond stress continues to increase with a small slip increase until the peak point. At this stage, bearing and friction dominate to resist the pull-out load in the case of specimens reinforced with GFRP (HW-SC) bars, whereas for the GFRP (SC) reinforced hinged beams, only friction resistance controls the response. The post – peak bond stress of the GFRP (type A) reinforced specimens that failed by pull-out only decayed gradually with increasing free end slip in a controlled ductile way. For hinged beams having 12.7 mm bar diameter with embedment length 10 d_b, their bond stress dropped suddenly with a sharp slip due to shear cracks subsequent to the pull-out failure. Also, the same softening trend occurred in specimens (A-15.9-10d_b-B/T), as a result of splitting cracks. The ascending curve was similar for all specimens having the same surface configuration. However, the descending curve varied with changing the failure mode. In addition, it was noted that the shape of bond stress – slip curve of GFRP (type A) bar changes with differing bar diameter. It may be attributed to the difference in the rib spacing with the bar diameter. While for the sand coated GFRP reinforced specimens, the bond failure was relatively brittle and bond stress decayed abruptly to be almost zero accompanied with a loud bang owing to stripping of sand coated layer. The post – peak bond stress starts again to increase up to a certain value with increasing in the slip due to remaining frictional resistance. This trend was observed for all hinged beams reinforced with GFRP (type B), except two specimens (B-9.5-5d-B and B-12.7-5d-T), where their softening branches reduced smoothly because of the partial detaching of sand coating. Also, the sudden decrease in bond stress was noticed in hinged beam (B-15.9-10d-B) due to shear failure. The residual stresses in GFRP (SC) reinforced hinged beams are lower than those in GFRP (HW-SC) reinforced hinged beams because of the full detachment of sand coated layer, leading to a smooth surface that was not able to provide with much frictional resistance. The slip corresponding to the maximum bond stress obtained from GFRP (type A) reinforced specimens is higher than that obtained from GFRP (type B) reinforced specimens, indicating that the amount of slip is influenced by the surface treatment. The effect of surface properties on the slip was also confirmed by Lee et al. [4] and Pepe et al. [24]. All specimens reinforced with steel bars exhibited high initial stiffness without a slip when chemical adhesion was dominated. Then, bond stress continued to increase with very little slip until failure. At this stage, mechanical interlock and friction controlled to resist the pull-out force. Unexpected failures occurred, the shear failure prior to the bond failure in specimens having embedment length $5d_b$ and yielding happened before de-bonding, following by shear crack in steel reinforced hinged beams having embedment length $10d_b$. Which in turn results in abruptly dropping the value of bond stress as shown in Figure 6.

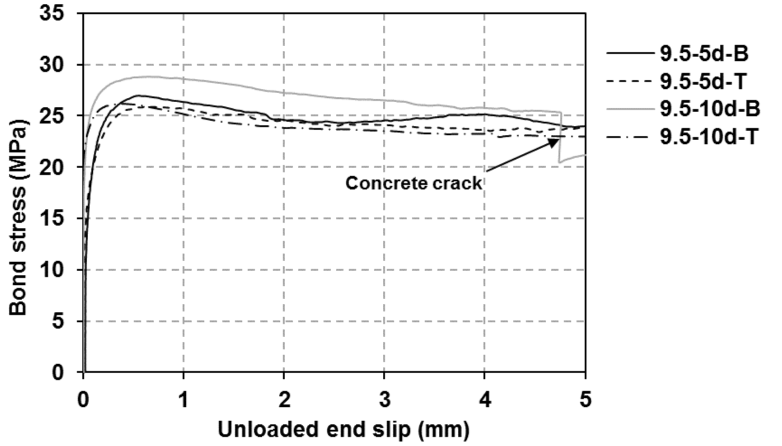

(a)

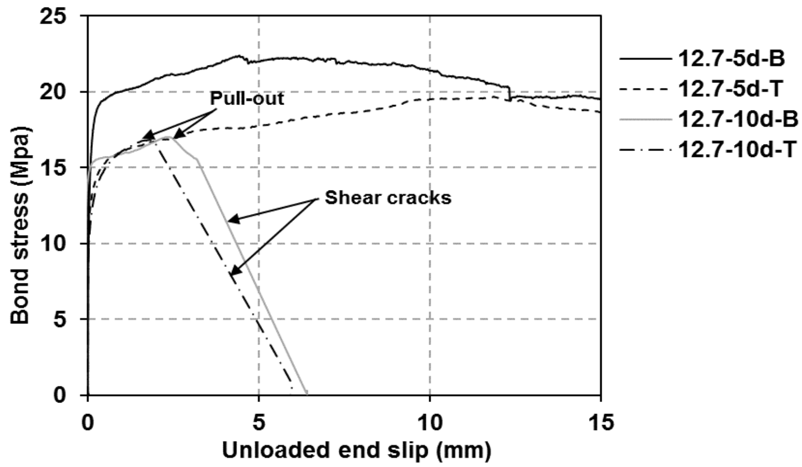

(b)

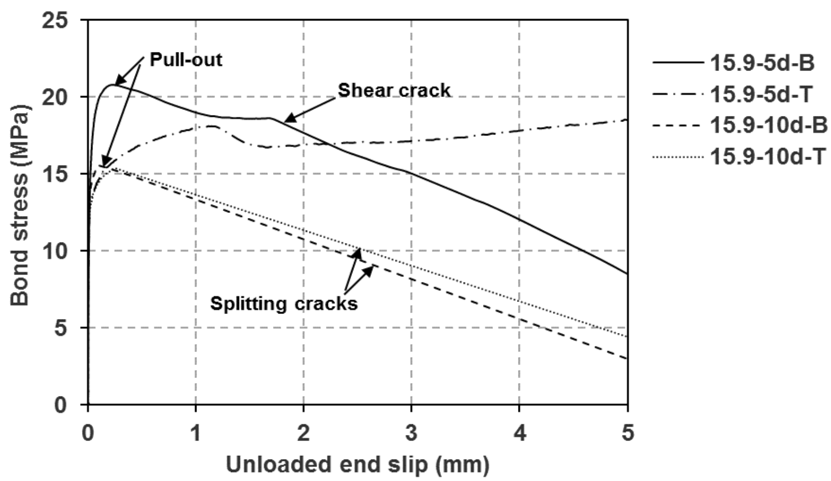

(c)

Figure 4. Bond stress versus free end slip for GFRP (HW-SC) bars

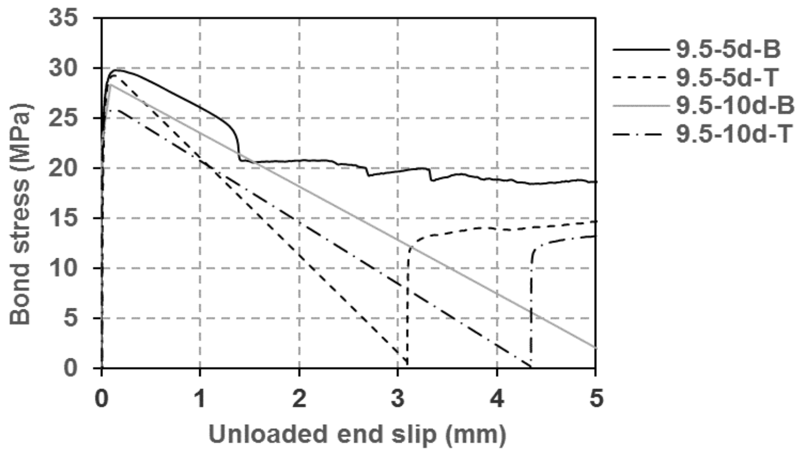

(a)

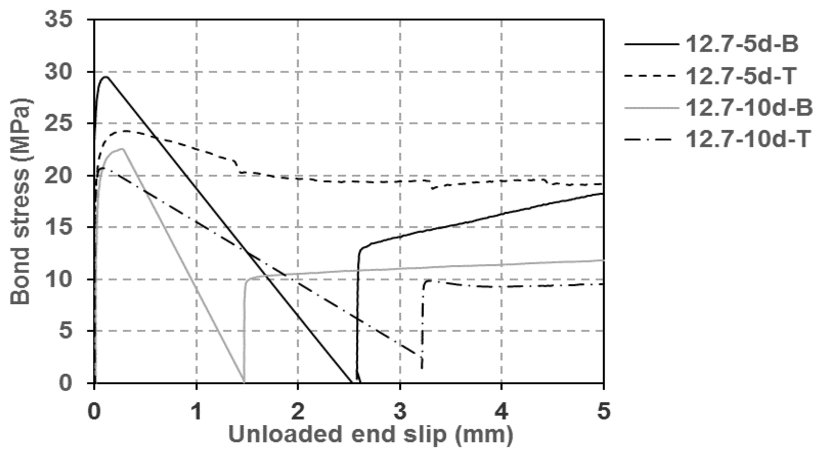

(b)

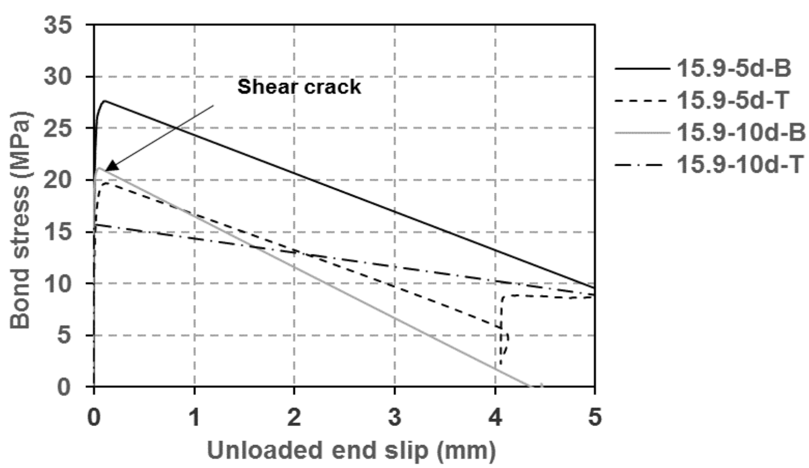

(c)

Figure 5. Bond stress versus free end slip for GFRP (SC) bars

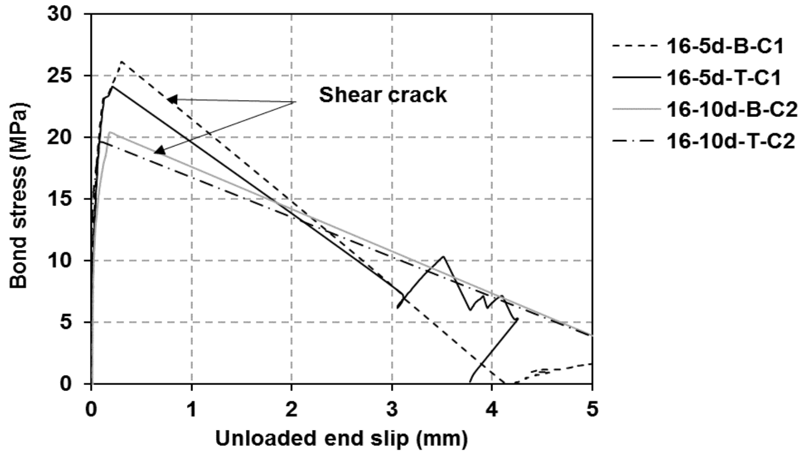

Figure 6. Bond stress versus free end slip for steel bars

3.2 Bond failure mechanism

The failure mode observed for each hinged beam is listed in Tables 2 and 3. Most specimens failed by a pull-out mode as shown in Figures 7 (a) and 8 (a), except the specimens reinforced with steel bars (C-16-5d-B/T) and specimen (B-15.9-10d-B) that failed by shear cracks as illustrated in Figure 8 (b and c). For specimens (A-15.9-10d-B/T), pull-out failure accompanied with splitting cracks was observed as indicated in Figure 7 (c). While the specimens (A-12.7-10d-B/T) and (A-15.9-5d-B) failed by a pull-out mode followed by narrow diagonal cracks as shown in Figure 7 (b). Steel reinforced hinged beams having embedment length $10d_b$ were failed by yielding subsequently shear crack.

The specimens were split after testing to visually assess the bar and surrounding concrete conditions. For helically wrapped with slightly sand coating GFRP reinforced specimens, some abrasions were noted on the outer layer with stripping of sand coated layer as described in Figure 9 (b). In addition, there was white residue on the trace of the whole embedment length, indicating crushing of resin. However, the specimens with longer embedment lengths failed by a damage of fibres as shown in Figure 9 (a). No apparent crushing of the surrounding concrete was monitored. As for specimens reinforced with sand coated GFRP bars, it was found that the concrete also remained uncrushed and sand grains detached completely as shown in Figure 9 (c), indicating that the bond strength between the outer layer and bar core is lower than that between the high-strength concrete and sand coating.

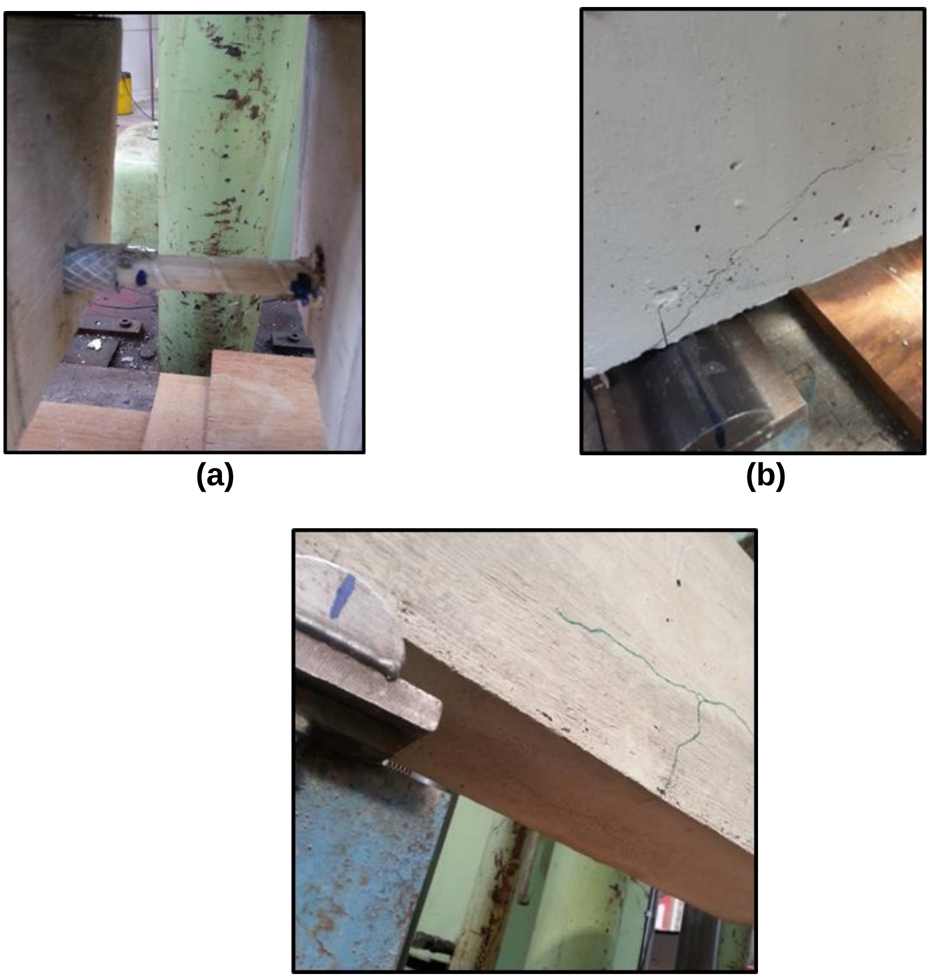

(a) (b) (c)

Figure 7. (a) Pull-out failure of GFRP (HW-SC) reinforced specimen, (b) Narrow shear cracks in specimen (A-12.7-10d-T/B) and (c) Splitting failure in specimen (A-15.9-10d-T/B)

(a)

(b)

(c)

Figure 8. (a) Pull-out failure of GFRP (SC) reinforced specimen, (b) Shear crack in specimen (B-15.9-10d-B) and (c) Shear failure in steel reinforced specimen

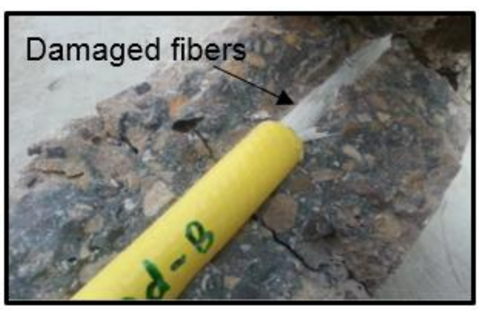

(a) Specimen (A-9.5-10d-B)

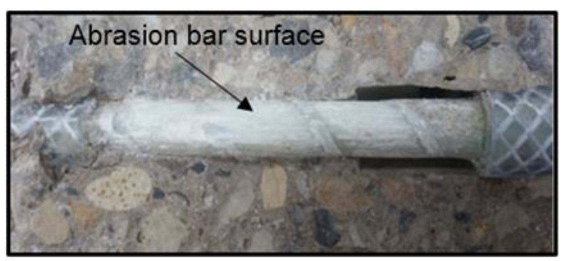

(b) Specimen (A-12.7-5d-B)

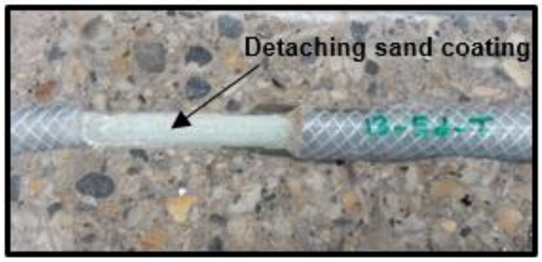

(c) Specimen (B-12.7-5d-T)

Figure 9. Visual inspection for the specimens failed by pull-out (images by author)

3.3 Factors influencing bond strength

3.3.1 Effect of embedment length on bond strength

In general, bond strength reduces with increasing bonded length as shown in Figures 10 and 11 because of non-linear distribution of bond stresses along the embedment length. This finding was confirmed by the results of Tighiouart et al. [8]. As the load increases, the bond stress at the vicinity of the unloaded end increases owing to the redistribution of shear stresses along the embedment length [7]. It is noticed that the reduction rate of bond strength of GFRP (HW-SC) reinforced specimens is approximately constant for all bar sizes, except for the 9.5 mm bar diameter. It is 24% and 15% for bottom and top bar positions, respectively. However, for GFRP (SC) reinforced specimens, the reduction rate of bond strength in smaller bar diameters is lower than that in larger bar diameters. It is in the range of 5% to 24% and 12% to 20% for the bottom and top bar positions, respectively. The bond strengths of sand coated and helically wrapped with slightly sand coated GFRP bars measured in the current investigation are much higher than those observed in the literature [7, 8] due to the high strength concrete of the current investigation and different surface configuration.

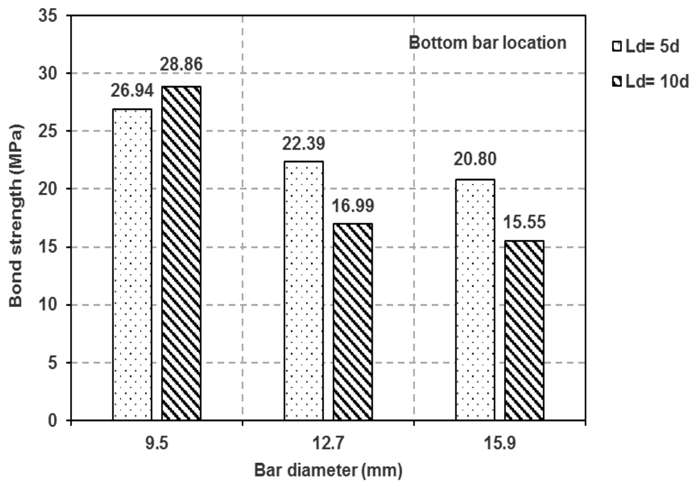

(a)

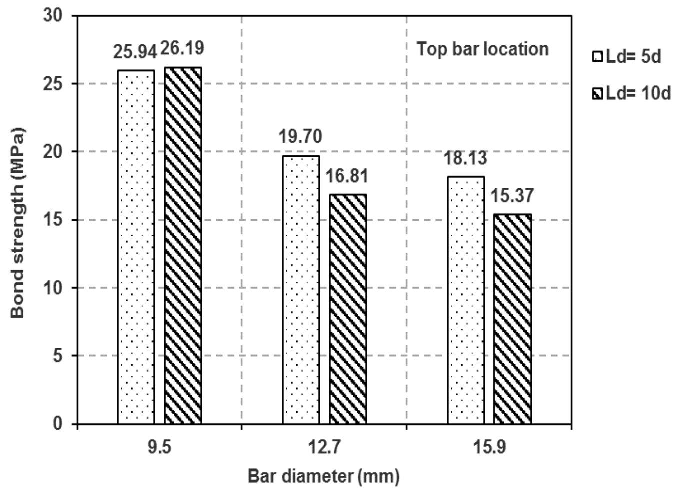

(b)

Figure 10. Effect of the embedment length and bar diameter on the average bond strength of GFRP (HW-SC) bars (a) Bottom bar position and (b) Top bar position

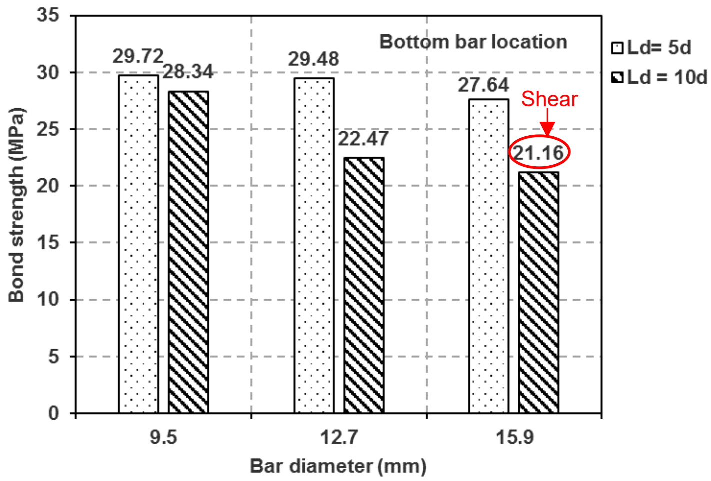

(a)

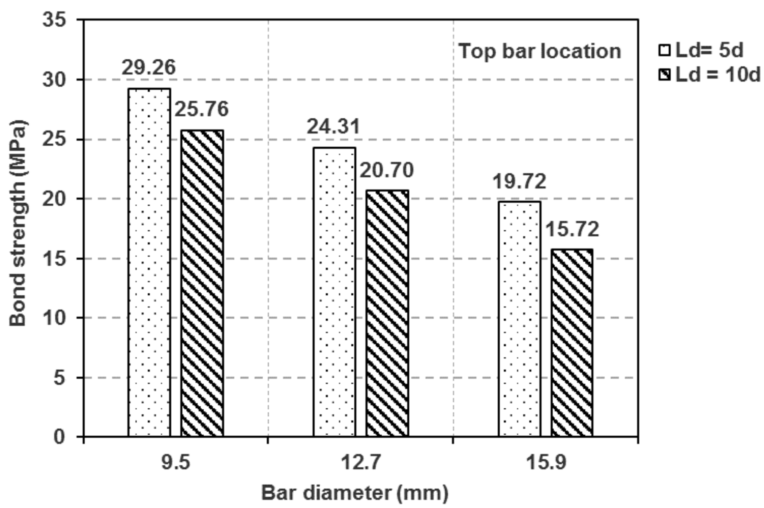

(b)

Figure 11. Effect of the embedment length and bar diameter on the average bond strength of GFRP (SC) bars (a) Bottom bar position and (b) Top bar position

3.3.2 Effect of bar diameter on bond strength

It can be seen from Figures 10 and 11 that the maximum bond strength increases for smaller bar diameters, agreeing with previous investigations on FRP and steel bars [2, 3, 7, 8, 25]. This phenomenon occurs due to bleeding of water underneath the bar, creating voids which in turn result in reducing the contact area between the bar and concrete [8]. The quantity of bleeding water trapped beneath larger bar diameters is greater than smaller ones. Therefore, the bond strength in larger bar diameters is lower than that in smaller bar diameters. For high strength concrete, the reduction rate in bond strength decreased with increasing bar diameter in GFRP (type A) reinforced specimens and bottom casting specimens reinforced with GFRP (type B) bars. The same conclusion was also reported by Lee et al. [5] for pull-out specimens. Whereas, a constant reduction rate in bond strength was observed in specimens having GFRP (type B) top bars.

3.3.3 Effect of bar position on bond strength

Figures 12 and 13 show the distribution of ratios of the maximum bond strength of the bottom bars to that of the top bars for both GFRP types. Top - cast bar specimens have bond strengths slightly lower than those of bottom - cast bar specimens because of a little bleeding water and a lower water / cement ratio, as reported by Pay et al. [15], Ferguson and Thompson [26] and Jirsa et al. [27]. It was observed that an average reduction in bond strength is 7 % and 15% for GFRP (Type A) and GFRP (Type B), respectively. The most significant reduction (14%) was measured in GFRP (HW-SC) reinforced specimens having 12.7 mm and 15.9 mm bar diameters and $5d_b$ embedment length. As the bonded length increased to $10d_b$, the ratio decreased leading to only a 1% strength reduction. While, it is 17% and 28% for GFRP (SC) reinforced specimens with 12.7 mm and 15.9 mm bar diameter, respectively, and $5d_b$ bonded length. This reduction in bond strength is owing to bleeding water and segregation close to the top layers of concrete. Therefore, the concrete surrounding the top bars is less consolidated compared to that surrounding the bottom bars, a similar conclusion was obtained by Chaallal and Benmokrane [12], Ehsani et. al [13], and Tighiouart et. al [8] from conducting the pull-out tests, and by Pay et. al [15] from testing lap-splice beams. Based on the experimental work carried out herein, the top – casting specimens produced a minor reduction in bond strength. Subsequently, these results obtained from top – casting specimens can be compared directly with those obtained from bottom – bar specimens. In the worst case, they will be slightly safe.

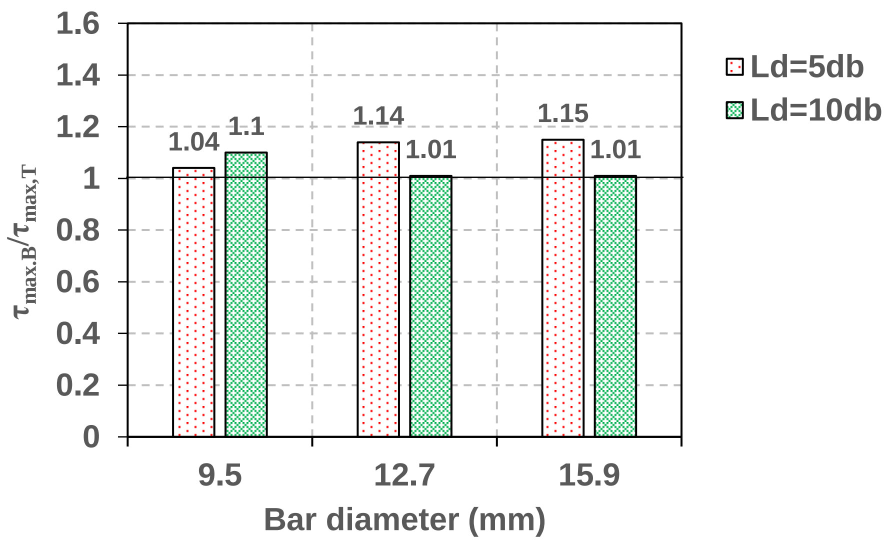

Figure 12. Comparison between bond strengths of GFRP (HW-SC) bottom bars and top bars

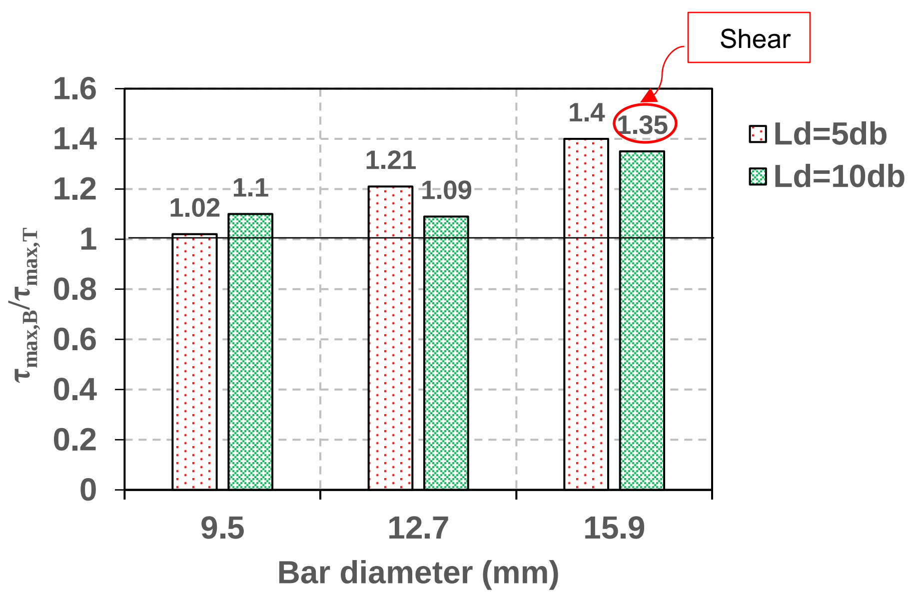

Figure 13. Comparison between bond strengths of GFRP (SC) bottom bars and top bars

3.3.4 Effect of bar surface on bond strength

From Figures 14 and 15, it can be seen that the bond strength of GFRP (SC) bars is higher than that of GFRP (HW-SC) bars owing to their sand coating surface. The ratio varied from 1.1 to 1.36 and from 1.02 to 1.23 based on bar diameter and embedment length for the bottom and top bars, respectively. However, the corresponding slip for GFRP (SC) surface is smaller than that for GFRP (HW-SC) surface as demonstrated in Tables 2 and 3. It can be reported that sand coating improves the bond performance better than helical wrapping as also reported by Cosenza et al. [28] and Davalos et al. [29]. However, Lee et al. [4] found that the bond strength of GFRP (HW-SC) bars is higher than that of GFRP (SC) bars for concrete strengths (25, 40 and 70 MPa) from testing pull-out specimens.

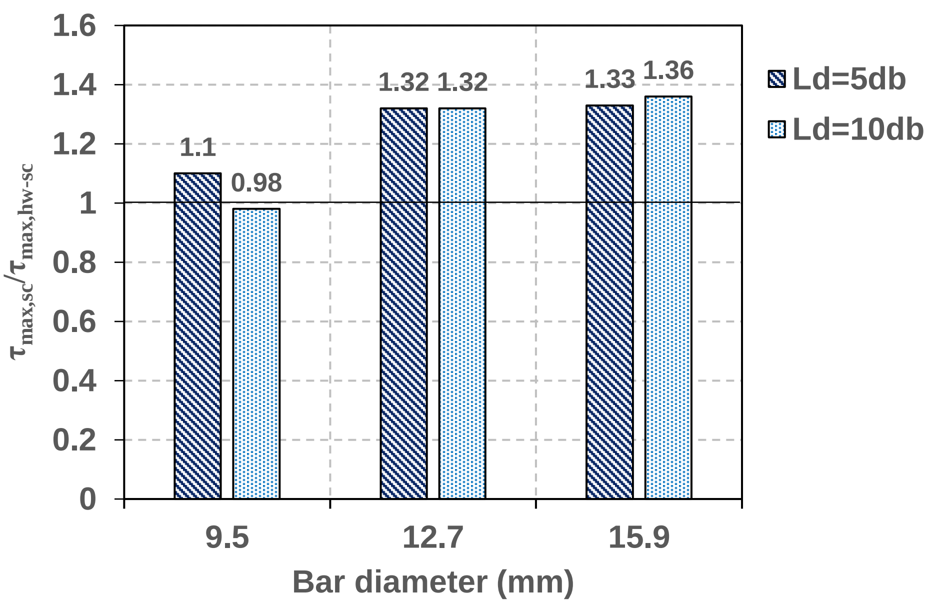

Figure 14. Comparison between bond strengths of GFRP (SC) and GFRP (HW-SC) surfaces for bottom bars

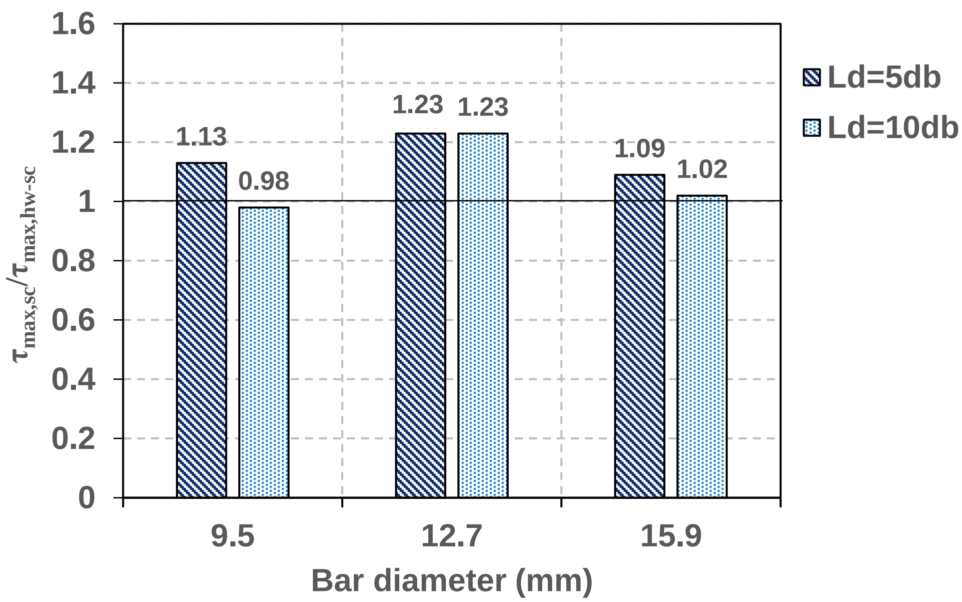

Figure 15. Comparison between bond strengths of GFRP (SC) and GFRP (HW-SC) surfaces for top bars

4. Comparison of test results with current codes

For comparison purposes, the bond strengths provided by code equations were determined based on the geometrical and mechanical properties of the hinged beams. The ACI 440.1R [22] code has derived an equation for GFRP bars based on the work conducted by Wambeke and Shield [30] as shown below:

$$\frac{\tau_{max}}{0.083\sqrt{f_c'}} = 4 + 0.3\frac{c}{d_b} + 100\frac{d_b}{l_e} \qquad (4)$$

where τ_{max} is the bond strength (MPa), f_c' is the cylinder compressive strength of concrete (MPa) and c is the lesser of the cover to the centre of the bar or one-half of the centre-to-centre spacing of the bars being developed (mm). The ratio of c/d_b is limited to be less than 3.5. The CAN/CSA-S806 [17] and CAN/CSA-S6 [18] Canadian codes have also proposed the expressions for estimating the development length of FRP bars in conventional concrete in order to avoid bond failure. These equations were substituted in equation 3 to produce the expressions 5 and 6 for CAN/CSA-S806 and CAN/CSA-S6, respectively, which are used to calculate bond strength.

$$\tau_{max} = \frac{\mathrm{d_{cs}}\sqrt{\mathrm{f_c'}}}{1.15\mathrm{k_1 k_2 k_3 k_4 k_5}\pi d_b} \tag{5}$$

$$\tau_{max} = \frac{\left(\mathrm{d_{cs}} + \mathrm{k_{tr}}\frac{\mathrm{E_{frp}}}{\mathrm{E_s}}\right)\mathrm{f_{cr}}}{0.45\mathrm{k_1 k_6}\pi d_b} \tag{6}$$

where:

$$k_{tr} = \frac{A_{tr} f_y}{10.5 s n} \qquad and \qquad \left(d_{cs} + k_{tr}\frac{E_{frp}}{E_s}\right) \leq 2.5 d_b$$

where $\mathbf{k_1}$ is a bar location factor (1.3 for horizontal reinforcement placed so that more than 300 mm of fresh concrete is cast below the development length or splice, 1.0 for other cases), $\mathbf{k_2}$ is a concrete density factor (1.3 for structural low-density concrete, 1.2 for structural semi-low-density concrete, 1.0 for normal density concrete), $\mathbf{k_3}$ is a bar size factor (0.8 for $A_b \leq 300$ mm^2, 1.0 for $A_b > 300$ mm^2), $\mathbf{A_b}$ is the cross-sectional area of FRP bar (mm^2), $\mathbf{k_4}$ is a bar fibre factor (1.0 for GFRP), $\mathbf{k_5}$ is a bar surface factor (1.0 for surface-roughened or sand-coated surfaces and 1.05 for spiral pattern surface), $\mathbf{k_6}$ is a bar surface factor, being the ratio of the bond strength of the FRP bar to that of a steel deformed bar with the same cross-sectional area as the FRP bar, but not greater than 1.0. In the absence of experimental data, k_6 shall be taken as 0.8, $\mathbf{d_{cs}}$ is the smaller of the cover to the centre of the bar or two-thirds of the centre-to-centre spacing of the bars being developed (mm) (not greater than 2.5 $\mathrm{d_b}$), $\boldsymbol{k_{tr}}$ is a transverse reinforcement index, $\boldsymbol{A_{tr}}$ is the cross-sectional area of transverse reinforcement (mm^2), **s** is maximum spacing centre to centre of transverse bars within l_d (mm), $\boldsymbol{f_{yt}}$ is yield stress in transverse reinforcement (MPa), **n** is the number of bars being developed along the potential plane of bond splitting, $\boldsymbol{f_{cr}}$ is the cracking strength of concrete (MPa) ($0.4\sqrt{f_c'}$ for normal-density concrete, $0.34\sqrt{f_c'}$ for semi-low-density concrete, $0.3\sqrt{f_c'}$ for low-density concrete), $\mathbf{E_{frp}}$ and $\mathbf{E_s}$ are the modulus of elasticity of FRP and steel bars, respectively. The square root of concrete strength should be less than 5 and 8 MPa for CSA-S806 and CSA-S6, respectively.

Tables 4 and 5 summarise the comparison of the experimental bond strength of various specimens and predictions using the methods provided in ACI 440.1R-15, CSA S806-12 and CSA S6-14. It can be seen that the ACI 440.1R code was more conservative for top-cast GFRP reinforced specimens than bottom-cast GFRP reinforced ones. The CSA S806 and CSA S6 codes are too conservative, where the average ratios of experimental to predicted bond strengths are 5.33 and 3.1 with a COV of 24% for GFRP (type A) bottom bars, respectively. Whereas, it is 4.95 and 2.88 with a COV of 23% for GFRP (type A) top bars, respectively. As for the GFRP (type B), the average ratios of experimental to predicted bond strengths are 6.37 and 3.89 with a COV of 11% for the bottom bars and 5.23 and 3.19 with a COV of 21% for the top bars. However, the average ratio of experimental to predicted bond strengths obtained from ACI 440 code is 1.52 and 2.13 with a COV of 34% for the bottom and top GFRP (type A) bars, respectively. While it is 1.98 with a COV of 24% for the bottom GFRP (type B) bars and 2.55 with a COV of 28% for the top GFRP (type B) bars. Tables 4 and 5 showed that the bond strength obtained by Canadian codes is not influenced by bar diameter and embedment length. CSA-S806 code considers the bond strength of helically wrapped surface is less (5%) than that of sand coating surface, while CSA-S6 recommended to use 0.8 for all surfaces, in absence the experimental data. Moreover, both Canadian codes neglect the effect of bar position on bond strength, as the depth of concrete underneath the bars is less than 300mm. Therefore, there is no change in bond strength with changing bar position as illustrated in Tables 4 and 5. The same observation was also confirmed by Hossain et al. [6]. In contrast to the Canadian codes, the bond strength reduces with increasing embedment length as per the ACI 440.1R code as shown in Figure 16 (a). In the ACI 440 equation, the effect of bar diameter on bond strength has been omitted by the normalized concrete cover and embedment length. In addition, the ACI 440. 1R code ignores the influence of surface configuration on bond strength. However, from tables 4 and 5, there is a slight increase in bond strength of GFRP (HW-SC) reinforced specimens compared to those reinforced with GFRP (SC) bars, because of a small variation of concrete strength. It is also noted from Figure 16 (a) that the predicted bond strength of the top bars is lower than that of the bottom bars, because the ACI 440. 1R code acknowledges the effect of bar position by a modification factor 1.5. The ACI 440.1R equation was developed based on concrete strength in the range of 28 to 45 MPa [30]. Therefore, it cannot be assumed to be accurate for predicting the bond strength of GFRP bar in HSC. The Canadian code limitations regarding concrete strength and concrete cover lead to a constant value of predicted bond strength for all test specimens as indicated in Figure 16 (b and c). Because of the absence of transverse reinforcement in hinged beams, the effect of confinement considered by transverse reinforcement index, k_{tr}, in the CSA S6 equation was neglected. The minimum value of the bond strength in experimental results is higher than the bond strengths obtained from Canadian design codes, thus, the development length provided by these codes will be over satisfactory.

Table 4. Comparison of test results of GFRP (type A) with different codes predictions

Specimen label	τ_{exp} (MPa)	ACI 440.1R τ_{pred} (MPa)	$\frac{\tau_{exp}}{\tau_{pred}}$	CSA-S806 τ_{pred} (MPa)	$\frac{\tau_{exp}}{\tau_{pred}}$	CSA-S6 τ_{pred} (MPa)	$\frac{\tau_{exp}}{\tau_{pred}}$
A-9.5-5d-B	26.94	18.23	1.42	4.11	6.55	7.07	3.81
A-9.5-10d-B	28.86	10.95	2.54	4.11	7.02	7.07	4.08
A-12.7-5d-B	22.39	18.23	1.18	4.11	5.45	7.07	3.17
A-12.7-10d-B	16.99	10.95	1.49	4.11	4.13	7.07	2.40
A-15.9-5d-B	20.80	18.16	1.10	4.11	5.06	7.07	2.94
A-15.9-10d-B	15.55	10.88	1.38	4.11	3.78	7.07	2.20
Average			1.52		5.33		3.10
COV%			34		24		24
A-9.5-5d-T	25.94	12.16	2.06	4.11	6.31	7.07	3.67
A-9.5-10d-T	26.19	7.30	3.46	4.11	6.37	7.07	3.70
A-12.7-5d-T	19.70	12.16	1.56	4.11	4.79	7.07	2.79
A-12.7-10d-T	16.81	7.30	2.22	4.11	4.09	7.07	2.38
A-15.9-5d-T	18.13	12.10	1.44	4.11	4.41	7.07	2.56
A-15.9-10d-T	15.37	7.25	2.04	4.11	3.74	7.07	2.17
C-16-5d-B	>26.07	N/A					
C-16-5d-T	>24.06	N/A					
Average			2.13		4.95		2.88
COV%			34		23		23

Note: τ_{exp} is the experimental bond strength; τ_{pred} is the predicted bond strength; COV is a Coefficient of variation and N/A = Not applicable.

Table 5. Comparison of test results of GFRP (type B) with different codes predictions

Specimen label	τ_{exp} (MPa)	ACI 440.1R τ_{pred} (MPa)	$\frac{\tau_{exp}}{\tau_{pred}}$	CSA-S806 τ_{pred} (MPa)	$\frac{\tau_{exp}}{\tau_{pred}}$	CSA-S6 τ_{pred} (MPa)	$\frac{\tau_{exp}}{\tau_{pred}}$
B-9.5-5d-B	29.72	17.33	1.71	4.32	6.88	7.07	4.20
B-9.5-10d-B	28.34	10.41	2.72	4.32	6.56	7.07	4.01
B-12.7-5d-B	29.48	17.33	1.70	4.32	6.82	7.07	4.17
B-12.7-10d-B	22.47	10.41	2.16	4.32	5.20	7.07	3.18
B-15.9-5d-B	27.64	17.26	1.60	4.32	6.40	7.07	3.91
B-15.9-10d-B	>21.16	10.34	N/A	4.32	N/A	7.07	N/A
Average			1.98		6.37		3.89
COV%			24		11		11
B-9.5-5d-T	29.26	11.55	2.53	4.32	6.77	7.07	4.14
B-9.5-10d-T	25.76	6.94	3.71	4.32	5.96	7.07	3.64
B-12.7-5d-T	24.31	11.55	2.10	4.32	5.63	7.07	3.44
B-12.7-10d-T	20.70	6.94	2.98	4.32	4.79	7.07	2.93
B-15.9-5d-T	19.72	11.50	1.71	4.32	4.56	7.07	2.79
B-15.9-10d-T	15.72	6.89	2.28	4.32	3.64	7.07	2.22
C-16-10d-B	>20.37	N/A					
C-16-10d-T	>19.65	N/A					
Average			2.55		5.23		3.19
COV%			28		21		21

Note: τ_{exp} is the experimental bond strength; τ_{pred} is the predicted bond strength; COV is a Coefficient of variation and N/A = Not applicable.

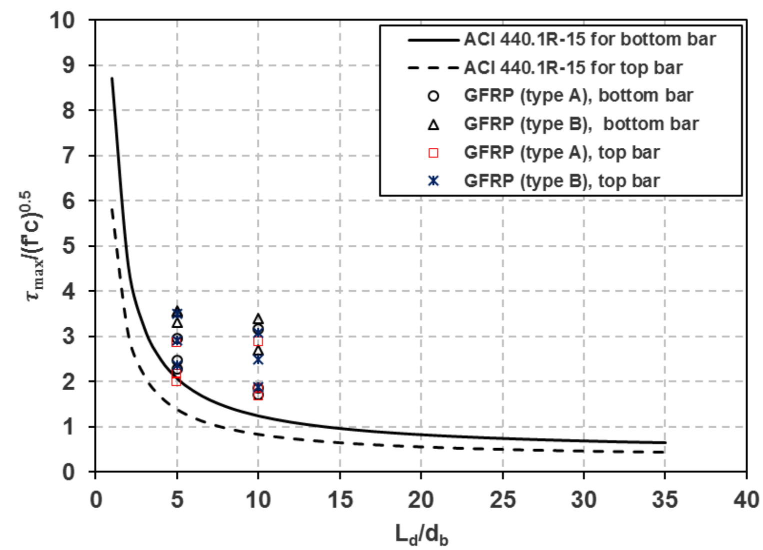

(a) Variation of maximum bond stress with embedment length

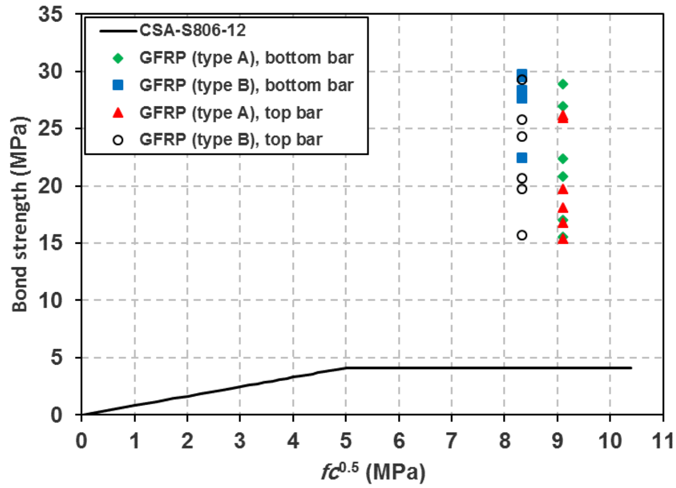

(b) Bond strength vs. square root of concrete strength

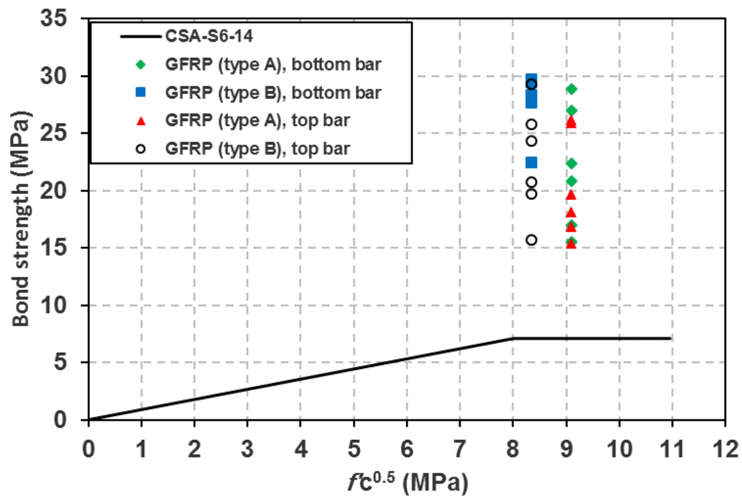

(c) Bond strength vs. square root of concrete strength

Figure 16. Comparison between predicted and experimental bond strengths

5. Conclusions

Test results of 28 HSC hinged beams reinforced with GFRP and steel bars have been presented and discussed in this paper. The parameters investigated were diameter, embedment length, surface configuration and position of reinforcing bars. The following conclusions are drawn:

1. Pull-out failure was observed in most specimens. Bond failure was governed by damage of the outer layer of GFRP (HW-SC) bars, while it was due to detachment of sand grains on the GFRP (SC) surface.
2. In the case of high strength concrete, after the peak bond stress, the GFRP (HW-SC) bars showed a gradual reduction in bond stresses due to friction resistance, whereas the GFRP (SC) bars showed sudden bond failure with complete loss of bond resistance because of stripping of the sand grains.
3. The bond strength of GFRP (SC) bars is higher than that of GFRP (HW-SC) bars. However, the corresponding slip for GFRP (SC) bars is less than that for GFRP (HW-SC) bars.
4. Bond strength reduces with increasing embedment length and bar diameter. For high strength concrete, the reduction rate in bond strength decreased with increasing bar size in all specimens, except top-cast specimens reinforced with GFRP (SC) bars having a constant reduction rate.
5. Top-cast specimens exhibited slightly lower bond strengths (average 7% and 15% reduction for GFRP (HW-SC) and GFRP (SC), respectively) than bottom-cast specimens.
6. CSA-S806 and CSA-S6 codes provide more conservative predictions of bond strengths of GFRP (HW-SC) and GFRP (SC) bars in high strength concrete than those provided by ACI 440.1R code

Acknowledgement

Authors would like to express their great appreciation and gratefully acknowledge to Ministry of Higher Education in Libya for funding this research work.

References

1. Achillides, Z. and K. Pilakoutas, Bond behavior of fiber reinforced polymer bars under direct pullout conditions. Journal of Composites for Construction, 2004. 8(2): p. 173-181.
2. Okelo, R. and R.L. Yuan, Bond strength of fiber reinforced polymer rebars in normal strength concrete. Journal of composites for construction, 2005. 9(3): p. 203-213.
3. Baena, M., et al., Experimental study of bond behaviour between concrete and FRP bars using a pull-out test. Composites Part B: Engineering, 2009. 40(8): p. 784-797.
4. Lee, J.Y., et al., Bond stress–slip behaviour of two common GFRP rebar types with pullout failure. Magazine of Concrete Research, 2012. 64(7): p. 575-591.
5. Lee, J.-Y., et al., Bond behaviour of GFRP bars in high-strength concrete: bar diameter effect. Magazine of Concrete Research, 2017. 69(11): p. 541-554.
6. Hossain, K.M.A., D. Ametrano, and M. Lachemi, Bond Strength of Standard and High-Modulus GFRP Bars in High-Strength Concrete. Journal of Materials in Civil Engineering, 2014. 26(3): p. 449-456.
7. Benmokrane, B., B. Tighiouart, and O. Chaallal, Bond strength and load distribution of composite GFRP reinforcing bars in concrete. ACI Materials Journal, 1996. 93(3): p. 246-252.
8. Tighiouart, B., B. Benmokrane, and D. Gao, Investigation of bond in concrete member with fibre reinforced polymer (FRP) bars. Construction and Building Materials, 1998. 12(8): p. 453-462.
9. Ovitigala, T. and M. Issa, Mechanical and Bond Strength of Basalt Fiber Reinforced Polymer (BFRP) Bars for Concrete Structures, in Proceedings of the 11th International Symposium on FRP for Reinforced Concrete Structures. Guimaraes, Portugal. 2013.
10. Xue, W., et al., Bond behavior of sand-coated deformed glass fiber reinforced polymer rebars. Journal of Reinforced Plastics and Composites, 2014. 33(10): p. 895-910.
11. Mazaheripour, H., et al., Experimental study on bond performance of GFRP bars in self-compacting steel fiber reinforced concrete. Composite Structures, 2013. 95: p. 202-212.
12. Chaallal, O. and B. Benmokrane, Pullout and bond of glass-fibre rods embedded in concrete and cement grout. Materials and structures, 1993. 26(3): p. 167-175.
13. Ehsani, M.R., H. Saadatmanesh, and S. Tao. Bond Behaviour and Design Recommendations for Fiberglass Reinforcing Bars. in Proceeding of the first International Conference on Composites in Infrastructure (ICCI-96). 1996b. Tucson, Ariz.
14. Benmokrane, B. and R. Masmoudi. FRP C-bar as reinforcing rod for concrete structures. in PROCEEDINGS OF THE 2ND INTERNATIONAL CONFERENCE ON ADVANCED COMPOSITE MATERIALS IN BRIDGES AND STRUCTURES, ACMBS-II, MONTREAL. 1996.
15. Pay, A.C., E. Canbay, and R.J. Frosch, Bond strength of spliced fiber-reinforced polymer reinforcement. ACI Structural Journal, 2014. 111(2): p. 257-266.

16. Golafshani, E.M., A. Rahai, and M.H. Sebt, Bond behavior of steel and GFRP bars in self-compacting concrete. Construction and Building Materials, 2014. 61: p. 230-240.
17. CAN/CSA-S806, Design and construction of building structures with fibre-reinforced polymers. 2012, Canadian Standards Association: Mississauga, Ontario, Canada.
18. CAN/CSA-S6, Canadian Highway Bridge Design Code. 2014, Canadian Standard Association.
19. ASTM-D7205/D7205M-06, Standard test method for tensile properties of fibre reinforced polymer matrix composite bars. 2006, ASTM International: West Conshohocken, United States. p. 13.
20. ASTM-A706/A706M-09b, Standard Specification for Low-Alloy Steel Deformed and Plain Bars for Concrete Reinforcement. 2009, ASTM International: West Conshohocken, United States. p. 6.
21. ACI-440.3R, Guide Test Methods for Fiber-Reinforced Polymers (FRPs) for Reinforcing or Strengthening Concrete Structures. 2012, ACI Committee 440: Farmington Hills, M1.
22. ACI-440.1R, Guide for the design and construction of concrete reinforced with FRP bars. 2015, ACI Committee 440: Farmington Hills, M1.
23. RILEM/CEB/FIP, R., RILEM technical recommendations for the testing and use of construction materials 1982, London : Spon, c1994. p. 213-217.
24. Pepe, M., et al., Numerical calibration of bond law for GFRP bars embedded in steel fibre-reinforced self-compacting concrete. Composites Part B: Engineering, 2013. 50: p. 403-412.
25. Achillides, Z., Bond behaviour of FRP bars in concrete, in Dept. of Civil and Structural Engineering. 1998, University of Sheffield: Sheffield, U.K.
26. Ferguson, P.M. and J.N. Thompson, Development Length of High Strength Reinforcing Bars in Bond. ACI Journal, 1962. 59(7): p. 887-922.
27. Jirsa, J.O., et al. Effect of casting position on bond. in International Conference on Bond in Concrete. 1982. Paisley College of Technology, Paisley, Scotland.
28. Cosenza, E., G. Manfredi, and R. Realfonzo, Behavior and modeling of bond of FRP rebars to concrete. Journal of composites for construction, 1997. 1(2): p. 40-51.
29. Davalos, J.F., Y. Chen, and I. Ray, Effect of FRP bar degradation on interface bond with high strength concrete. Cement and Concrete Composites, 2008. 30(8): p. 722-730.
30. Wambeke, B.W. and C.K. Shield, Development length of glass fiber-reinforced polymer bars in concrete. ACI Structural Journal, 2006. 103(1): p. 11-17.